Inorganic Chemistry

Article

pubs.acs.org/IC

$Ga_4B_2O_9$: An Efficient Borate Photocatalyst for Overall Water Splitting without Cocatalyst

Guangjia Wang,[†] Yan Jing,[†] Jing Ju,[‡] Dingfeng Yang,[†] Jia Yang,[†] Wenliang Gao,[†] Rihong Cong,*[,†] and Tao Yang*[,†]

[†]College of Chemistry and Chemical Engineering, Chongqing University, Chongqing 400044, People's Republic of China

[‡]Beijing National Laboratory for Molecular Sciences, College of Chemistry and Molecular Engineering, Peking University, Beijing 100871, People's Republic of China

Supporting Information

ABSTRACT: Borates are well-known candidates for optical materials, but their potentials in photocatalysis are rarely studied. Ga^{3+}-containing oxides or sulfides are good candidates for photocatalysis applications because the unoccupied 4s orbitals of Ga usually contribute to the bottom of the conducting band. It is therefore anticipated that $Ga_4B_2O_9$ might be a promising photocatalyst because of its high Ga/B ratio and three-dimensional network. Various synthetic methods, including hydrothermal (HY), sol–gel (SG), and high-temperature solid-state reaction (HTSSR), were employed to prepare crystalline $Ga_4B_2O_9$. The so-obtained HY-$Ga_4B_2O_9$ are micrometer single crystals but do not show any UV-light activity unless modified by Pt loading. The problem is the fast recombination of photoexcitons. Interestingly, the samples obtained by SG and HTSSR methods both possess a fine micromorphology composed of well-crystalline nanometer strips. Therefore, the excited e^- and h^+ can move to the surface easily. Both samples exhibit excellent intrinsic UV-light activities for pure water splitting without the assistance of any cocatalyst (47 and 118 μmol/h/g for H_2 evolution and 22 and 58 μmol/h/g for O_2 evolution, respectively), while there is no detectable activity for P25 (nanoparticles of TiO_2 with a specific surface area of 69 m^2/g) under the same conditions.

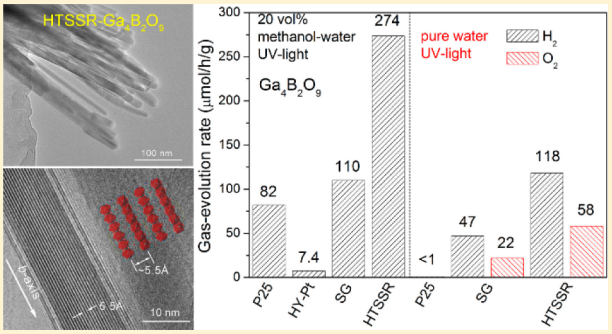

INTRODUCTION

Hydrogen is an environmentally friendly and high-capacity energy carrier. Photoinduced water splitting can convert solar energy to the chemical form of H_2, but it is not a spontaneous process and catalysts are required. Since 1972, massive efforts have been devoted to TiO_2-based photocatalysts.[1] In addition, investigations for efficient photocatalysts have been extended to other semiconducting oxides, sulfides, oxynitrides, and so on.[2−6]

Metal borates are well-known for optical applications, like nonlinear optical crystals and luminescent materials.[7−9] Researchers have not paid enough attention to their photocatalytic performances. Only a few examples have been reported. For instance, $InBO_3$ can photocatalyze the degradation of 4-chlorophenol;[10] CuB_2O_4 and $Cu_3B_2O_6$ (by loading Pt as the cocatalyst) can catalyze water splitting under visible-light irradiation;[11] $Bi_4B_2O_9$ and $Bi_2O_2[BO_2(OH)]$ show observable visible-light activities for methylene blue degradation;[12] the nonlinear optical material $K_3B_6O_{10}Br$ shows good catalytic activity in UV-induced dechlorination of chlorophenols;[13] very recently, an open-framework gallium borate, $Ga_9B_{18}O_{33}(OH)_{15}\cdot H_3B_3O_6\cdot H_3BO_3$ (Ga-PKU-1), has been reported as a UV-light photocatalyst for water reduction, however, requiring the assistance of sacrificial regents.[14]

In Ga-PKU-1, the bottom of the conducting band (CB) is mainly contributed by 4s orbitals of Ga.[14] $Ga_4B_2O_9$, another gallium borate with a higher Ga/B ratio, attracted our attention. It is natural to anticipate that the density of states (DOS) of the CB would be higher in $Ga_4B_2O_9$ than in Ga-PKU-1. The structure of $Ga_4B_2O_9$, which is quite complex and shows the coexistence of ordering and disordering of polyhedra connections (see Figure S1 in the Supporting Information, SI), was first solved by a powder X-ray diffraction (XRD) technique in 2009.[15] As a mullite derivate, GaO_6 octahedra share edges to form chains along the *b* axis, and the chains are cross-linked by GaO_5, BO_3, and BO_4 groups. It is reasonable that the three-dimensional connectivity of Ga–O polyhedra offers pathways for the migration of e^- and h^+. Accordingly, we expect an outstanding photocatalytic activity for this borate candidate $Ga_4B_2O_9$.

On the other hand, researchers are seeking materials that can extensively absorb visible-light photons and catalyze water splitting without sacrificial reagents.[16] It is particularly difficult to catalyze the overall water splitting because the photogenerated e^- and h^+ easily recombine before they could react

Received: January 2, 2015
Published: February 25, 2015

DOI: 10.1021/ic5031087
Inorg. Chem. 2015, 54, 2945−2949

with substrates. As a result, catalysts on the nanoscale are favorable, which can significantly reduce the length for photogenerated excitons moving to the surface, and nanocrystals also provide a higher specific area and hence more active sites than bulk materials.[17] Here in our work, we proposed that the wide-gap semiconductor $Ga_4B_2O_9$ is an intrinsic and efficient photocatalyst for pure water splitting without any cocatalyst; for instance, the H_2-evolution rate is 118 μmol/h/g when $Ga_4B_2O_9$ was prepared in the form of straight nanostrips with diameter of <20 nm.

EXPERIMENTAL SECTION

Synthesis. Three synthetic methods, including hydrothermal (HY), sol–gel (SG), and high-temperature solid-state reaction (HTSSR), were employed to prepare $Ga_4B_2O_9$.

HY method: β-Ga_2O_3 is the gallium source. First, a prereaction was performed to dissolve Ga_2O_3 (2.5 mmol, 0.4686 g) using concentrated HNO_3 in a closed system (180 °C, 10 h). The resultant solution evaporated to near dryness by gentle heating of the container. Thereafter, 0.3 mol of H_3BO_3 was charged, and the system was sealed again and maintained at 240 °C for another 5 days. Transparent needlelike single crystals were obtained after washing unwanted residuals.

SG method: 1 mmol of β-Ga_2O_3 (0.1874 g) was dissolved using the above method. Then the solution, together with 2 mmol of H_3BO_3, and an appropriate amount of citric acid were charged into 50 mL of water. The mixture was heated gently with continuous stirring for 2 h to remove the excess water. The resulting gel precursor was dried in an oven at 180 °C and then preheated at 500 °C for 10 h with a temperature ramp rate of 1 °C/min. After grinding in an agate mortar, the prescursor was further calcined in air at 620 °C for 10 h. The resultant powder was slightly gray and was washed with water to remove the possible excessive boric acid. The gray powder was further heated at 620 °C again for 5 h under dynamic O_2 flow to oxidize the residual C. Finally, it became white and was ready for catalytic evaluation.

HTSSR method: 1 mmol of β-Ga_2O_3 (0.1874 g) was dissolved using the above method. We allowed the solution to evaporate naturally without heating. Then, the resultant white solid was mixed with 2 mmol of H_3BO_3 in an agate mortar and calcined at 590 °C for 10 h. The final powder was also washed carefully.

The compounds prepared using the above-mentioned methods are denoted as HY-, SG-, and HTSSR-$Ga_4B_2O_9$, respectively.

Characterizations. Powder XRD was performed on a PANalytical X'pert diffractometer with Cu Kα radiation at 40 kV and 40 mA. Le Bail refinements were performed using the software package *TOPAS*.[18] Transmission electron microscopy (TEM; JEOL JEM-2100F) was employed to observe the morphologies of as-prepared materials at an accelerating voltage of 200 kV. The UV–vis light absorption spectra were recorded at room temperature using a Shimadzu UV-3600 spectrometer equipped with an integrating sphere attachment. $BaSO_4$ was used as a reflectance standard. The band gaps were estimated according to the peak in the differential curve of the absorption spectra. The specific surface area determination was performed by the Brunauer–Emmett–Teller (BET) method with N_2 adsorption at 77 K using a Quantachrome Quadrasorb SI analyzer. Prior to the measurements, samples were degassed at 300 °C for 48 h.

Photocatalytic Reactions. We used a gas-closed circulation system equipped with a vacuum line (CEL-SPH2N system; see Figure S2 in the SI), a reaction vessel, and a gas sampling port that was directly connected to a gas chromatograph. In a typical run, 0.050 g of photocatalyst was used. A total of 50 mL of an aqueous solution, together with the catalyst, was added into a 150 mL reaction vessel with a quartz cover. The solution was kept stirring, and a 10 °C recycling water bath was applied to keep the reaction vessel at a constant temperature. For the UV-light source, a 500 W Hg lamp was used. All of the $Ga_4B_2O_9$ samples used in our work were stable after the photoirradiation experiments, showing no changes in their powder XRD patterns (see the details in the SI).

Theoretical Calculations. Theoretical studies on $Ga_4B_2O_9$ were operated by the Vienna Ab Initio Simulation Package.[19] The projector augmented-wave method,[20] implemented in the VASP code, was utilized to describe the interaction between the ionic cores and valence electrons. The generalized gradient approximation parametrized by Perdew, Burke, and Ernzerhof[21] was employed to describe the exchange-correlation potential in the standard density functional theory calculations. For single-point energy and DOS, a cutoff energy of 400 eV for the plane-wave basis and 4 × 11 × 6 Monkhorst–Pack G-centered k-point meshes were employed. The band structures E(k) were computed on a discrete k mesh along with high-symmetry directions.

RESULTS AND DISCUSSION

The phase purity of three as-made $Ga_4B_2O_9$ samples was verified by powder XRD. As shown in Figure S3 in the SI, Le Bail refinements were performed to estimate their cell parameters, which are all consistent with each other. In addition, the very sharp peak shape for the sample prepared by the HY method indicates its good crystallinity. It can be seen from the scanning electron microscopy (SEM) photograph (see Figure S4 in the SI), where HY-$Ga_4B_2O_9$ is made up of microcrystals. The other two samples show obviously diffused peaks, which is a typical sign of poor crystallinity. This difference in crystallinity was indeed confirmed through the measurements of the specific surface areas, as shown in Figure 1. Both SG- and HTSSR-$Ga_4B_2O_9$ possess significantly higher

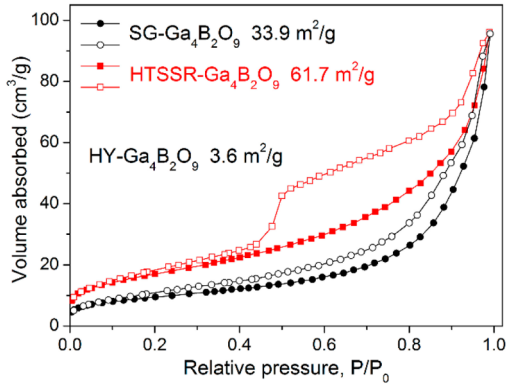

Figure 1. N_2 adsorption–desorption curves at 77 K. The filled and open symbols represent the adsorption and desorption branches, respectively. The specific surface areas are estimated by the BET method.

BET surface areas than HY-$Ga_4B_2O_9$; especially, the HTSSR sample has a substantial loop at the high relative pressure region. In fact, the nanotype morphology for the SG and HTSSR samples is the main interest point of this work and will be discussed in a later section.

The UV–vis absorption spectra for three as-prepared $Ga_4B_2O_9$ are shown in Figure 2, where the band gaps are estimated to be ~4.46 and 4.12 eV, respectively. The relatively narrower band gap for HTSSR-$Ga_4B_2O_9$ endows it with better absorption ability to photons, which may enhance its photocatalytic performance among these three samples.

We first evaluated the photocatalytic property of HY-$Ga_4B_2O_9$. It is somehow disappointing that no detectable photocatalytic activity to water reduction was observed for HY-$Ga_4B_2O_9$, even by using the sacrificial reagent CH_3OH.

DOI: 10.1021/ic5031087
Inorg. Chem. 2015, 54, 2945–2949

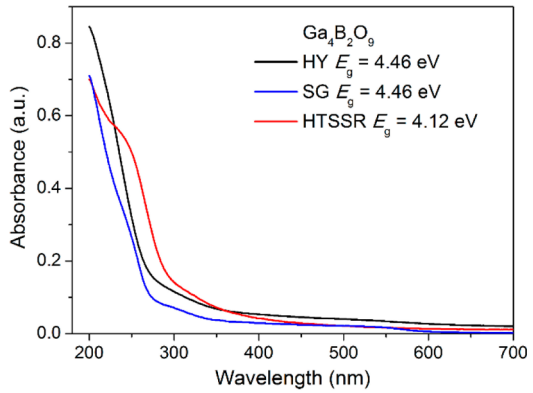

Figure 2. UV−vis reflectance spectra for various $Ga_4B_2O_9$ samples.

Therefore, a simple post-treatment of 1 wt % Pt loading was employed, and eventually an observable H_2-production rate of 7.4 μmol/h/g was detected (see Figure 3); however, the

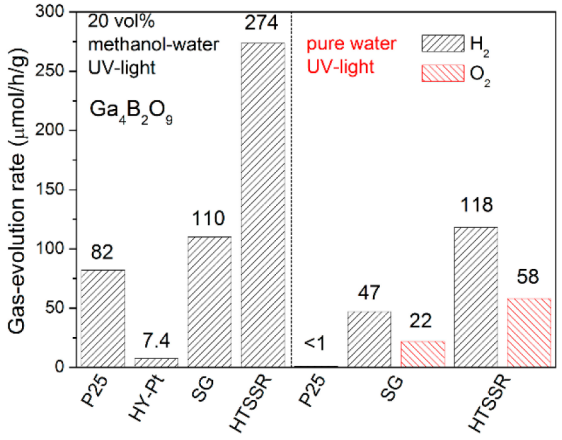

Figure 3. Photocatalytic gas evolution rate for various $Ga_4B_2O_9$ samples under different conditions. P25 was used as the reference catalyst. Detailed gas evolution curves against irradiation time are included in the SI.

efficiency is only 9% P25 (TiO_2 nanoparticles) in a CH_3OH−H_2O system. Nevertheless, this first attempt at least confirms that $Ga_4B_2O_9$ is intrinsically photoresponsive. The problem should be the very short lifetime of photogenerated e^- and h^+.

It is well-known that the micromorphology is very important to the performance of a heterogeneous catalyst. Researchers usually make great efforts to increase the specific surface area, or the total amount of activity sites (by exposing appropriate crystalline facets).[22−25] Therefore, two additional synthetic methods were employed to prepare $Ga_4B_2O_9$ catalysts, including the SG and HTSSR methods.

For SG-$Ga_4B_2O_9$, numerous nanorods with dimensions of about tens of nanometers are severely agglomerated (see Figure 4a). More importantly, the nanorods are well crystallized, and the majority of the crystals grow along *a* or *c* axis (see Figure 4b). In other words, the exposed surface is mostly correlated with the *ac* crystal planes, which are perpendicular to the direction of GaO_6-octahedral chains (Figure S1 in the SI). The band gap is 4.46 eV, the same as that of its bulk form (HY-$Ga_4B_2O_9$). The specific surface area is as high as 33.9 m^2/g, which is about 9.4 times higher than that of micrometer single crystals (3.6 m^2/g). Therefore, the photocatalytic H_2-generation rate in an aqueous methanol solution is greatly

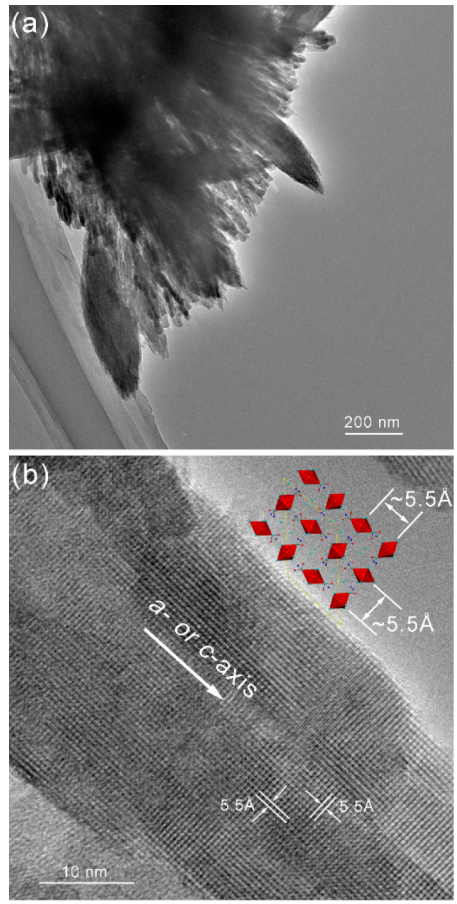

Figure 4. (a) Low- and (b) high-magnification TEM images for SG-$Ga_4B_2O_9$. The high-resolution image shows the orientation of the nanorods that grow along the *a* or *c* axis.

enhanced to 110 μmol/h/g, without using Pt as the cocatalyst (see Figure 3).

Such an increase of the catalytic activity from bulk to nanocrystals is reasonable. First, the inner part of the bulk particles usually cannot be irradiated by the incident beam, while it should not a big problem for the nanocrystals. Second, the photoexcited e^- can easily migrate to the surface in the SG sample, and probably the highly uniform orientation of the nanocrystals can reduce the chance of charge recombination. Third, a high specific surface area provides more active sites to capture water molecules for further reactions.

The HTSSR method used here is slightly different from the traditional process for synthesizing oxides. We use $Ga(NO_3)_3$ (by dissolving β-Ga_2O_3 in HNO_3) as the raw material, which reacts with excessive H_3BO_3. The so-obtained HTSSR-$Ga_4B_2O_9$ has a beautiful morphology (see Figure 5), which consist of straight nanostrips of hundreds of nanometers in length and <20 nm in diameter. These nanostrips are well crystallized and possess very smooth surfaces. More importantly, the high-resolution TEM image shows that these nanocrystals grow along the *b* axis (the direction of GaO_6-octahedral chains; Figure S1b in the SI), and therefore the exposed facets are perpendicular to those in SG-$Ga_4B_2O_9$. The BET surface is 62 m^2/g, and the band gap is decreased to 4.12 eV (see Figures 1 and 2). The H_2-evolution rate reaches 274 μmol/h/g, much higher than that of P25. There are several reasons for this further increase of activity. First, the exposed facets are different from those in SG-$Ga_4B_2O_9$ and are quite smooth, thus showing

DOI: 10.1021/ic5031087
Inorg. Chem. 2015, 54, 2945−2949

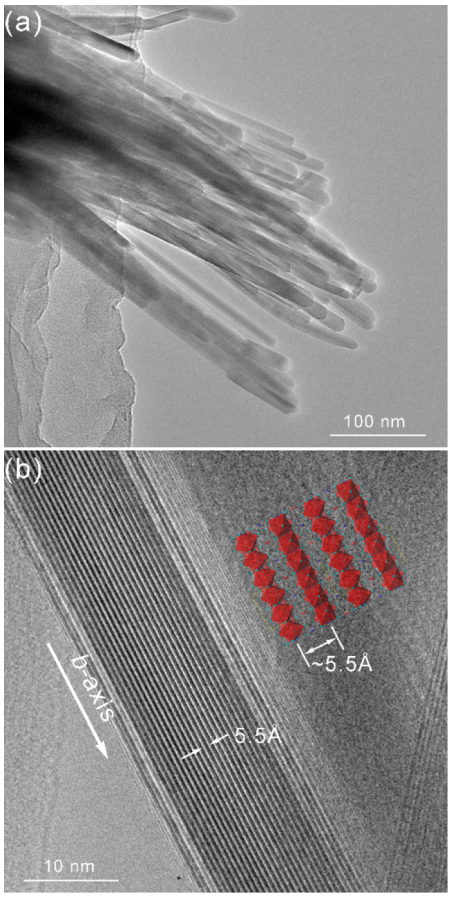

Figure 5. (a) Low- and (b) high-magnification TEM images for HTSSR-$Ga_4B_2O_9$. The high-resolution image clearly shows that the *b* axis is the easy growth axis for the nanostrips.

no steric hindrance effect for binding with substrate species. Second, the narrowing of the band gap allows more photons to be absorbed by HTSSR-$Ga_4B_2O_9$. Third, the very small diameters of these nanostrips can further reduce the average migration length for photogenerated e^- to react with water molecules.[16,22−25] Additionally, the long nanostrips are not as severely agglomerated in the HTSSR sample as in the SG sample.

Using sacrificial agents is helpful to elongate the lifetime of photogenerated e^- and h^+; however, it is not economic and therefore unwanted in practical applications. In our study, we observed very high levels of photocatalytic efficiency for both SG- and HTSSR-$Ga_4B_2O_9$ because of their high specific surface areas and significantly short pathways for e^-/h^+ to move to the surface. Indeed, both SG- and HTSSR-$Ga_4B_2O_9$ can catalyze pure water splitting without any cocatalyst and sacrificial agent, for example, 47 and 118 μmol/h/g for H_2 evolution, 22 and 58 μmol/h/g for O_2 evolution, respectively, under UV light (see Figure 3), while under the same experimental conditions, H_2 generation catalyzed by P25 (with a BET surface of 69 m^2/g) is below the detecting limit (<1 μmol/h/g) even after long-term irradiation. As a new photocatalyst, its stability during the catalyst process was also studied. HTSSR-$Ga_4B_2O_9$ kept its activity after four photocatalytic cycles, and XRD shows no obvious degradation (see Figure S5 in the SI).

As mentioned in the Introduction, the very complex structure of $Ga_4B_2O_9$, showing the coexistence of ordering and disordering arrangements of polyhedra (see Figure S1 in the SI), hampers an accurate calculation of its electronic structure. Nevertheless, we constructed an ordered structure model by doubling the periodic length along the *c* axis (as shown in Figure 6a), in order to better understanding the

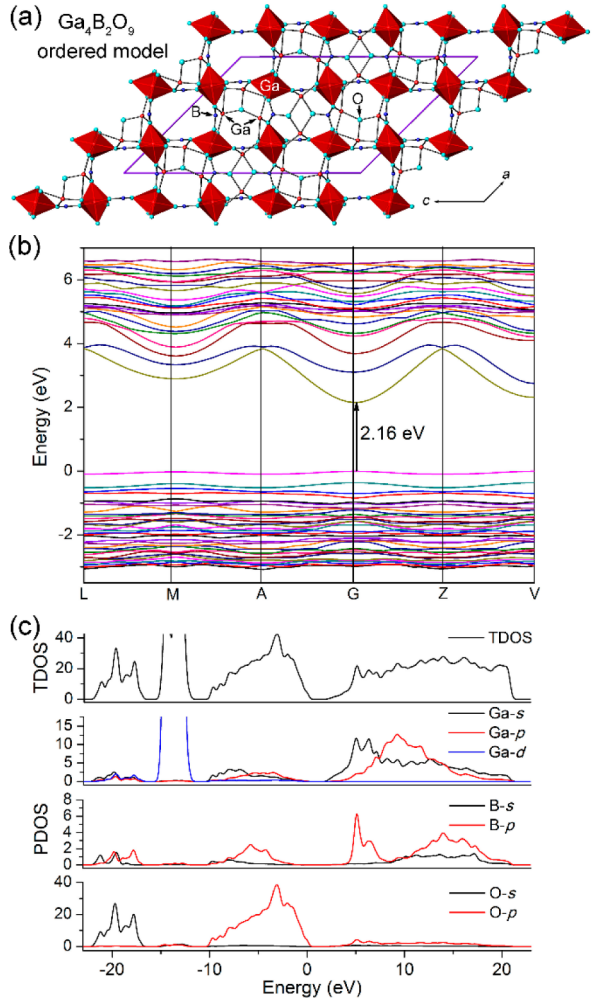

Figure 6. (a) Ordered structural model of $Ga_4B_2O_9$ constructed for theoretical calculations by doubling the *c* axis, (b) electronic band structure, and (c) DOS of $Ga_4B_2O_9$ in such an ordered model.

photocatalytic behavior theoretically within a reasonable approximation. As shown in Figure 6b, the calculated electronic band structure of $Ga_4B_2O_9$ along the symmetry lines in the Brillouin zones suggests a direct band gap of 2.16 eV. Usually a calculated band gap is smaller than the experimental value because of the discontinuity of the XC energy. Moreover, the bottom of the CB at G point shows a deep dispersion, which usually suggests a light effective mass of photoexcited e^-. On the contrary, the orbitals of the valence band (VB) are relatively flat, suggesting a slow mobility of h^+. In other words, such a band structure would cause a large difference in the respective mobility of photoexcited e^- and h^+ and eventually be beneficial to an efficient charge separation.

As shown in Figure 6c, it is expected that the VB maxima were mostly contributed by the 2p orbitals of O. The CB minimum was determined by the 4s orbitals of Ga. The 2p orbitals of B also partially contribute to both VB and CB. Accordingly, we could reasonably anticipate that the photo-

DOI: 10.1021/ic5031087
Inorg. Chem. 2015, 54, 2945−2949

current was conducted along the three-dimensional network composed of $Ga^{3+}-O^{2-}$ ionic bonds.

It is also interesting that micrometer single crystals of HY-$Ga_4B_2O_9$ show no activity due to the dynamic problem. Morphology control of this candidate by employing various synthetic methods is critical. As a result, we observe significant enhancement of the catalytic performances for the SG and HTSSR samples, even in a pure water system and without any noble-metal loading. The morphology engineering is vital to shortening the e^-/h^+ pathways to the surface and suppressing their recombination. We propose to pay particular attention to utilizing various synthetic methods for synthesizing metal borates.

CONCLUSION

In conclusion, we employed three synthetic methods to prepare micrometer and nanometer crystalline $Ga_4B_2O_9$ samples. The noble-metal-free nanostrips for SG- and HTSSR-$Ga_4B_2O_9$ show excellent UV-light activities for pure water splitting, while there is no detectable activity for P25 under the same conditions. Until now, studies on borate photocatalysts have been really scarce, and our observation of $Ga_4B_2O_9$ represents an excellent example that metal borates can catalyze the overall water splitting efficiently, without the assistance of any cocatalyst and sacrificial reagents. There are hundreds of structure types in the borate family; thus, it is promising to discover new photocatalysts by looking at photoresponsive metal borates with similar structural features.

ASSOCIATED CONTENT

Supporting Information

Crystal structure views of $Ga_4B_2O_9$, photograph of the photocatalytic evaluation setup used in our work, powder XRD, SEM images, H_2- and O_2-evolution curves against irradiation time. This material is available free of charge via the Internet at http://pubs.acs.org.

AUTHOR INFORMATION

Corresponding Authors

*E-mail: congrihong@cqu.edu.cn.
*E-mail: taoyang@cqu.edu.cn.

Notes

The authors declare no competing financial interest.

ACKNOWLEDGMENTS

This work was financially supported by the Nature Science Foundation of China (Grants 21101175, 21171178, 91222106, and 21201012) and Natural Science Foundation Project of Chongqing (Grants 2012jjA0438 and 2014jcyjA50036). We also acknowledge support of the open fund from Beijing National Laboratory for Molecular Sciences (Grant 20140155).

REFERENCES

(1) Fujishima, A.; Honda, K. *Nature* **1972**, *238*, 37−38.
(2) Chen, X. B.; Shen, S. H.; Guo, L. J.; Mao, S. S. *Chem. Rev.* **2010**, *110*, 6503−6570.
(3) Shen, S. L.; Wang, Q. B. *Chem. Mater.* **2013**, *25*, 1166−1178.
(4) Hisatomi, T.; Kubota, J.; Domen, K. *Chem. Soc. Rev.* **2014**, *43*, 7520−7535.
(5) Lu, D. L.; Takata, Y.; Saito, N.; Inoue, Y.; Domen, K. *Nature* **2006**, *440*, 295.
(6) Lee, Y.; Teramura, K.; Hara, M.; Domen, K. *Chem. Mater.* **2007**, *19*, 2120−2127.
(7) Becker, P. *Adv. Mater.* **1998**, *10*, 979−992.
(8) Pan, S. L.; Smit, J. P.; Watkins, B.; Marvel, M. R.; Stern, C. L.; Poeppelmeier, K. R. *J. Am. Chem. Soc.* **2006**, *128*, 11631−11634.
(9) Szczeszak, A.; Grzyb, T.; Barszcz, B.; Nagirnyi, V.; Kotlov, A.; Lis, S. *Inorg. Chem.* **2013**, *52*, 4934−4940.
(10) Yuan, J. X.; Wu, Q.; Zhang, P.; Yao, J. H.; He, T.; Cao, Y. *Environ. Sci. Technol.* **2012**, *46*, 2330−2336.
(11) Liu, J. K.; Wen, S. H.; Zou, X. X.; Zuo, F.; Beran, G. J. O.; Feng, P. Y. *J. Mater. Chem. A* **2013**, *1*, 1553−1556.
(12) Huang, H. W.; He, Y.; Lin, Z. S.; Kang, L.; Zhang, Y. H. *J. Phys. Chem. C* **2013**, *117*, 22986−2294.
(13) Fan, X. Y.; Zhang, L.; Zhang, M.; Qiu, H. S.; Wang, Z.; Yin, J.; Jia, H. Z.; Pan, S. L.; Wang, C. Y. *Chem. Mater.* **2014**, *26*, 3169−3174.
(14) Gao, W. L.; Jing, Y.; Yang, J.; Zhou, Z. Y.; Yang, D. F.; Sun, J. L.; Lin, J. H.; Cong, R. H.; Yang, T. *Inorg. Chem.* **2014**, *53*, 2364−2366.
(15) Cong, R. H.; Yang, T.; Li, K.; Li, H. M.; You, L. P.; Liao, F. H.; Wang, Y. X.; Lin, J. H. *Acta Crystallogr., Sect. B* **2010**, *66*, 141−150.
(16) Kudo, A.; Miseki, Y. *Chem. Soc. Rev.* **2009**, *38*, 253−278.
(17) Ran, J. R.; Zhang, J.; Yu, J. G.; Jaroniec, M.; Qiao, S. Z. *Chem. Soc. Rev.* **2014**, *43*, 7787−7812.
(18) *TOPAS, V4.1-beta*; Bruker AXS: Karlsruhe, Germany, 2004.
(19) Kresse, G.; Joubert, D. *Phys. Rev. B* **1999**, *59*, 1758.
(20) Blochl, P. E. *Phys. Rev. B* **1994**, *50*, 17953.
(21) Perdew, J. P.; Burke, K.; Ernzerhof, M. *Phys. Rev. Lett.* **1996**, *77*, 3865.
(22) Shen, S. L.; Wang, Q. B. *Chem. Mater.* **2013**, *25*, 1166−1178.
(23) Wu, C. Z.; Feng, F.; Xie, Y. *Chem. Soc. Rev.* **2013**, *42*, 5157−5183.
(24) Sun, Y. F.; Gao, S.; Xie, Y. *Chem. Soc. Rev.* **2014**, *43*, 530−546.
(25) Kuang, Q.; Wang, X.; Jiang, Z. Y.; Xie, Z. X.; Zheng, L. S. *Acc. Chem. Res.* **2014**, *47*, 308−318.

DOI: 10.1021/ic5031087
Inorg. Chem. 2015, 54, 2945−2949